

A Comparative Study of Layered Transition Metal Oxide Cathodes for Application in Sodium-ion Battery

Ivana Hasa^a, Daniel Buchholz^{b,c}, Stefano Passerini^{b,c*} and Jusef Hassoun^{a,*}

a Department of Chemistry, “Sapienza” University of Rome, Piazzale Aldo Moro, 5, 00185 Rome, Italy

b Helmholtz Institute Ulm, Helmholtzstraße 11, 89081 Ulm, Germany.

c Karlsruhe Institute of Technology (KIT), PO Box 3640, 76021 Karlsruhe, Germany

* jusef.hassoun@uniroma1.it, stefano.passerini@kit.edu

Abstract

Herein we report a study on P-type layered sodium transition metal-based oxides with general formula Na_xMO_2 ($\text{M}=\text{Ni}, \text{Fe}, \text{Mn}$). We synthesize the materials via co-precipitation followed by annealing in air and water rinsing process and examine the electrodes as cathodes for sodium-ion battery using a propylene carbonate (PC) based electrolyte. Following, we fully investigate the effect of Ni to Fe ratio, annealing temperature and sodium content on the electrochemical performances of the electrodes. The impact of these parameters on the structural and electrochemical properties of the materials is revealed by X-ray diffraction, scanning electron microscopy and cyclic voltammetry, respectively. The suitability of this class of P-type materials for sodium battery application is finally demonstrated by cycling tests revealing an excellent electrochemical performance in terms of delivered capacity, i.e. of about 200 mAh g^{-1} , and charge-discharge efficiency, approaching 100 %.

Keywords

Na_xMO_2 ($\text{M}=\text{Ni}, \text{Fe}, \text{Mn}$); Cathode; P2-P3-type layered structure; sodium-ion, battery.

Introduction

Nowadays, energy conversion and storage is one of the great challenges of mankind. Hence, efficient, safe, low cost and environmentally friendly storage systems are required in response to the modern society needs. Li-ion batteries (LIBs) are considered one of the promising systems to fulfill these requirements. In fact, they represent the most widespread secondary battery for consumer and portable electronics and are also considered very promising candidates for power hybrid and electric vehicles.^{1,2} Nevertheless, the market as well as the application for rechargeable batteries are highly diversified and various requirements have to be fulfilled. Stationary energy storage in contrast to high energy applications is mainly driven by cost efficient energy storage, which already points out that alternative battery chemistries complementary to and not competing with the lithium-ion battery technology are necessary.^{3,4} Sodium-ion batteries have the potential to fulfill this criteria and match the economic and environmental issues due to the high abundance and low cost of the employed materials.^{5,6}

Research on sodium-ion based batteries has been conducted in parallel with lithium systems at the beginning of the 1980's⁷⁻¹⁰, however the superior electrochemical performances led to a focus on LIBs. New Na-ion systems has attracted the interest of the broad scientific community again, with particular attention devoted to the study of intercalation and insertion materials. Indeed, suitable, high performance cathodes and alternative anodes instead of the reactive metallic sodium have been discovered.¹¹⁻¹⁵

Considering the large ionic radius of sodium and its preference for 6-fold coordination, like octahedral or prismatic, poly-anionic networks and layered oxides so far appeared to be the most appropriate positive active materials so far. Research on the intercalation chemistry of sodium into layered oxides with the general formula Na_xMO_2 (M=transition metal) started around 1980¹⁶, in which also the classification of the structure according to the stacking arrangement of the metal oxide layers was developed¹⁷. These layered materials consist of MO_6 edge-sharing octahedral units forming $(\text{MO}_2)_n$ sheets, in between which the sodium cation is coordinated octahedral (O), tetrahedral (T) or prismatic (P). O-type layered oxides

comprise sodium ions in octahedral sites, while P-type materials accommodate the alkali ions in prismatic sites. The most common structures for layered sodium-based transition metal oxides are of O3, P2 and P3-type, whereby the number indicates the number of transition metal layers in the repeating cell unit.^{16,17} Transition metal layered oxides have attractive properties as cathode materials for sodium-ion batteries, such as the ease of the synthesis and the high feasibility and reversibility of the sodium shuttling process, thus, allowing a good overall electrochemical performance.¹⁸

Among the cathode candidates, single transition-metal layered oxides Na_xMO_2 ($\text{M}=\text{V}, \text{Cr}, \text{Mn}, \text{Fe}, \text{Co}, \text{Ni}$)¹⁹⁻²³ have been studied although the initial investigations resulted in poor specific capacity and low retention. It has been demonstrated that nanostructured materials in combination with proper electrolyte solutions may be a valid approach to overcome the above mentioned issues.²⁴⁻²⁷ Furthermore, it has been reported that the intermixing of transition-metals in the MO_2 -sheets improves the structural stability and electrochemical cycling performance. Indeed, these substituted layered sodium-based oxides represent suitable electrode materials for the use in sodium-ion batteries.²⁸⁻³⁰ Manganese and iron based materials are of particular interest due to the high elemental abundance and low cost, as well as the promising performance of the electrodes including them as doping elements. In addition, also nickel is known to be very beneficial for the electrochemical performance, e.g., due to the $\text{Ni}^{2+}/\text{Ni}^{4+}$ redox process³⁰ but, yet, no detailed study has been performed on how its content affects the electrochemical properties of Na_xMO_2 ($\text{M}=\text{Ni}, \text{Fe}, \text{Mn}$). Herein, we present a comparative study on the impact of the Ni:Fe ratio, annealing temperature and stoichiometric sodium content during synthesis on the structural, morphological and electrochemical properties of various layered compounds of the type Na_xMO_2 ($\text{M}=\text{Ni}, \text{Fe}, \text{Mn}$). Target of this study is to reveal how the parameter affect the materials properties or, by implication, how different materials can be synthesized by varying these parameters, which is valuable for the development of the synthesis and the design of layered cathode materials for SIBs.

Experimental

Material synthesis and characterization

All the samples were synthesized by a solid-state reaction between sodium hydroxide (NaOH pellets Sigma Aldrich > 98%) and nickel-iron-manganese precursors. The precursors were prepared by co-precipitation method.³⁰ Accordingly, stoichiometric proportions of NiSO₄·6H₂O (Sigma Aldrich, ACS reagent 99%), FeSO₄·7H₂O (AnalaR NORMAPUR, analytical reagent), and MnSO₄·5H₂O (AnalaR NORMAPUR, analytical reagent) were dissolved in water according to the desired Ni/Fe ratio content. An aqueous solution of NaOH (50% excess) was added drop-wise in order to obtain the precursors. After extensive washing with distilled water, the precursors [Ni_xFe_yMn_z](OH)₂ were dried over night at 120°C. After grinding, the precursors were mixed with 0.685 equivalents of sodium precursor (NaOH powder from grinded NaOH pellets). The mixtures were pre-annealed in air atmosphere at 500°C for 5 hours (5°C/min). All materials have been subjected to a final thermal treatment at 900°C for 5 hours (5°C/min) followed by a water rinsing process. The layered compounds general formula was Na_xNi_yFe_zMn_{0.66}O₂, and the materials were differing by Ni/Fe ratio. Following these conditions, five materials have been characterized, i.e. Na_{0.6}Ni_{0.22}Fe_{0.11}Mn_{0.66}O₂, Na_{0.6}Ni_{0.155}Fe_{0.155}Mn_{0.66}O₂, Na_{0.5}Ni_{0.11}Fe_{0.22}Mn_{0.66}O₂, Na_{0.5}Ni_{0.05}Fe_{0.255}Mn_{0.66}O₂ and Na_{0.4}Fe_{0.33}Mn_{0.66}O₂.

Additionally, Na_{0.6}Ni_{0.22}Fe_{0.11}Mn_{0.66}O₂, was prepared at annealing temperature of 900 °C, 850°C and 800 °C, in order to check the influence of the thermal treatment on the material structure. The synthesis of the Na_{0.6}Ni_{0.22}Fe_{0.11}Mn_{0.66}O₂ at 800 °C was repeated also by changing the amount of initial sodium precursor from 0.685 equivalent to 1eq. Afterward, all the materials (NFMs compounds) were subjected to a water treatment (1 g of material was stirred in 100 mL of distilled water at 25°C for 5 min).^{29,30} Finally, all the obtained materials were dried at 120°C for 24 hours, grinded and stored under inert atmosphere. We may assume, considering the synthesis conditions (high temperature in air atmosphere) and literature data that the oxidation state of the transition metals are (+II), (+III) and (+IV) respectively

for Ni, Fe and Mn. The sodium content and the transition metal ratio in the samples were detected by inductively coupled plasma optical emission spectrometry with a Spectro ARCOS ICP-OES (Spectro Analytical Instruments, Kleve, Germany) instrument with axial plasma viewing.

The crystalline structure of the samples was detected by X-ray diffraction (XRD, Bruker D8 Advance, Germany) using the Cu K α radiation in the 2θ range from 10° to 90° .

Field emission scanning electron microscopy analysis (FE-SEM, Zeiss Auriga) was performed to get a morphological overview.

Electrochemical characterization

Electrodes were prepared by mixing the active material (85 wt. %) with carbon black (Super C65, TIMCAL, 10 wt. %) and polyvinylidene fluoride PVdF, (6020 Solef, Arkema Group, 5 wt. %). The slurries were made by adding appropriate amount of N-methyl-2-pyrrolidone (NMP). After 2 hours of intimate mixing, the resulting slurry was cast onto Al foil and dried at 120°C . Punching and pressing of the electrodes (12 mm diameter) has followed. The mass loading of the electrodes was about 3mg cm^{-2} (2.55mg cm^{-2} active material). Sodium metal was used as counter and reference electrodes. The sodium was cut from sodium pieces (99.8%, Acros Organics), pressed and finally punched on the current collector.

The electrodes were assembled into Swagelok-type sodium cells with 1M NaPF $_6$ in PC as electrolyte solution, which was soaked into a glass fiber (Whatman) separator. Cells were assembled in an argon-filled glove box with a H $_2$ O and O $_2$ content lower than 1 ppm. Cyclic voltammetry tests were performed using a scan rate of 0.1 mV s^{-1} in the 4.6V-1.5V (vs Na/Na $^+$) potential range at $20^\circ\text{C}\pm 2^\circ\text{C}$ using a VMP multichannel potentiostatic-galvanostatic system (Biological Science Instrument, France). The cells were cycled galvanostatically at 15 mA g^{-1} within 4.6V-1.5V voltage range at $20^\circ\text{C}\pm 2^\circ\text{C}$ using Maccor series 4000 battery tester (U.S.A).

Result and discussion

Figure 1 gives an overview on the structural and morphological properties of the five NFM samples with different Ni:Fe ratio via X-Ray Diffraction (XRD) and Field Emission Scanning Electron Microscopy (FE-SEM). The X-ray diffraction patterns reveal that all materials are characterized by a layered, P2-type structure belonging to the hexagonal $P6_3/mmc$ space group (ICSD-93469). The patterns corresponding to $\text{Na}_{0.6}\text{Ni}_{0.22}\text{Fe}_{0.11}\text{Mn}_{0.66}\text{O}_2$, $\text{Na}_{0.6}\text{Ni}_{0.155}\text{Fe}_{0.155}\text{Mn}_{0.66}\text{O}_2$ and $\text{Na}_{0.5}\text{Ni}_{0.11}\text{Fe}_{0.22}\text{Mn}_{0.66}\text{O}_2$ in Fig.1 (a), (b) and (c), respectively, reveal the absence of crystalline impurities. Further decrease of nickel content, with corresponding increase of the iron content, is accompanied by the appearance of a reflection at lower angles in the patterns of $\text{Na}_{0.5}\text{Ni}_{0.05}\text{Fe}_{0.255}\text{Mn}_{0.66}\text{O}_2$ and $\text{Na}_{0.4}\text{Fe}_{0.33}\text{Mn}_{0.66}\text{O}_2$, reported in figure 1(d) and (e), respectively. These peaks can be attributed to the presence of the hydrated phases caused by the water rinsing process, intend to dissolve sodium carbonate impurities formed during the annealing process but also leading to a partial chemical de-sodiation. In fact, it has been demonstrated that water can intercalate into the layered structure, which is leading to an increase of the interlayer distance and causing a shift of the $(00l)$ reflections to lower angles. Accordingly, the two diffraction peaks at 14° and 28° , which are marked by asterisks in Figure 1(d) and (e), may be indexed as $(002')$ and $(004')$, respectively.^{31,32} The presence of intercalated water can be explained considering the lower amount of sodium within compounds with higher content of Fe.

Indeed, a lower amount of sodium results in increased repulsion of neighbouring oxygen layers. Water intercalation during the rinsing process takes place to reduce the overall energy. The water intercalation, however, is not energetically favoured for larger sodium contents. Furthermore, it cannot be excluded that the absence of shifted reflections in the samples with increased Ni content (XRD in Fig.1a, b and c) may be attributed to the Ni-superlattice ordering action that hinders the water intercalation upon rinsing.^{31,33} The FE-SEM images reported as insets of the X-ray diffractograms in Fig. 1, clearly show the well-defined morphology typical of layered structure, characterized by a series of

planes forming a single particles with an average dimension ranging from 1 to 2 μm . The figure shows the presence of trace impurities of sodium carbonates, minor differences in particle size and negligible effects of the intercalated water in the samples with lower Ni content. Furthermore, the above-mentioned Ni-superlattice ordering effect (samples in Fig. 1a, b and c) allows a well-defined layered structure, more pronounced in respect to the other samples.

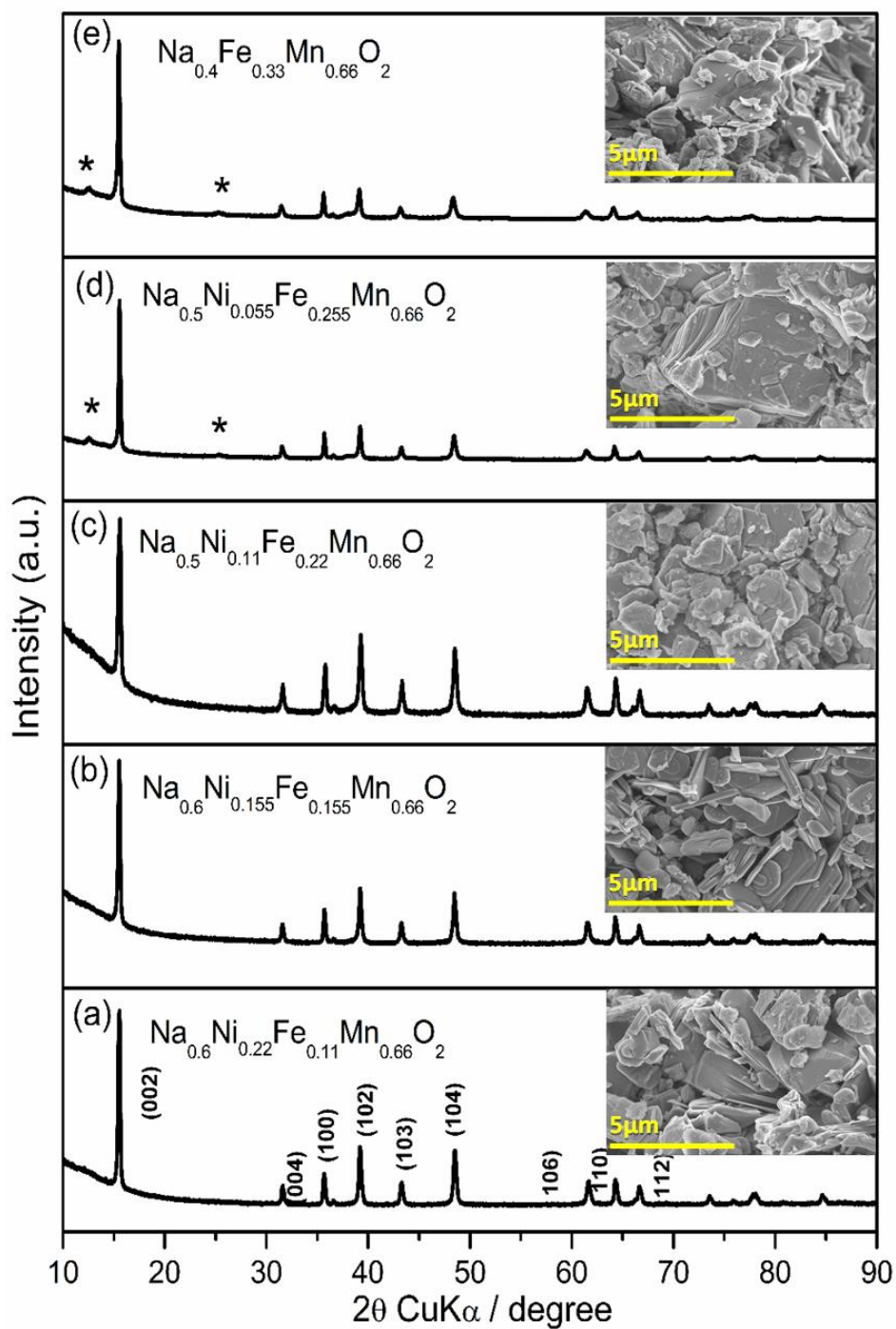


Figure 1. XRD patterns and FE-SEM images (insets) of P2-type NFM compounds with different Ni to Fe ratio. (a) $\text{Na}_{0.6}\text{Ni}_{0.22}\text{Fe}_{0.11}\text{Mn}_{0.66}\text{O}_2$, (b) $\text{Na}_{0.6}\text{Ni}_{0.155}\text{Fe}_{0.155}\text{Mn}_{0.66}\text{O}_2$, (c) $\text{Na}_{0.5}\text{Ni}_{0.11}\text{Fe}_{0.22}\text{Mn}_{0.66}\text{O}_2$, (d) $\text{Na}_{0.5}\text{Ni}_{0.05}\text{Fe}_{0.255}\text{Mn}_{0.66}\text{O}_2$, (e) $\text{Na}_{0.4}\text{Fe}_{0.33}\text{Mn}_{0.66}\text{O}_2$.

Figure 2a reports the cyclic voltammetry tests (CV) of the various NaNFM samples in sodium half cells, performed to study the influence of the Ni/Fe ratio on the electrochemical behaviour of the electrode. The voltammograms show the typical peaks associated to the electrochemical sodium (de)intercalation process into the layered structure, involving reversible processes in the 2V-4V potential region and phase change at the higher potential values. All samples exhibit a reversible redox process at about 2.0V vs. Na/Na⁺, i.e. higher sodium contents, due to the Mn⁴⁺/Mn³⁺ redox process and corresponding structural rearrangement of the layers^{34,35} and the two-phase oxidation reaction associated with the formation of the O2-phase, resulting from the gliding of the layers at very low sodium content (4.2 V vs. Na/Na⁺).¹³ The sample with the higher nickel content (Na_{0.6}Ni_{0.22}Fe_{0.11}Mn_{0.66}O₂ in panel I) shows the reversible peaks between 3.2 V and 3.9 V vs. Na/Na⁺, attributed to the Ni²⁺/Ni⁴⁺ redox couple, with a double-electron process involving changes in the layer alignment in the material and structural reorganization due to sodium vacancy ordering, with consequent change in the peak shape and final stabilization upon cycling (see region marked by the green circle in panel I). Following, panels II, III and IV evidence that the progressive increase of the Fe content, and the corresponding decrease of the Ni content, leads to the shift of the peaks associated to the above mentioned Ni²⁺/Ni⁴⁺ redox process to lower voltage (see region marked by the green dotted-line in panel I to IV). As expected, the Ni-free sample (Na_{0.6}Fe_{0.33}Mn_{0.66}O₂ in panel V) does not show peaks in the 3.2-3.9V potential region but the appearance of reversible peaks at lower voltage, i.e. around 3V, most likely due to the Fe²⁺/Fe³⁺ redox couple (see regions marked by the red circle in panel V and by the corresponding red dotted-line). Furthermore, the voltammograms reveal that an increasing Fe content leads to an increase of the intensity and a slight shift to lower voltages of the peak corresponding to the Mn⁴⁺/Mn³⁺ redox process at 2V. This is due to the charge compensation which implies an increased amount of redox active manganese at lower Ni²⁺ contents. We can reasonably assume that Ni doping stabilizes the material due to a minor Mn³⁺ formation with consequent improvement of the energy efficiency of the (de)-sodiation process. The suitability of

the P2-NFMs as cathode materials is verified in terms of galvanostatic cycling in sodium metal half cells. Figure 2 (b) reports the voltage profiles and cycling behavior of the different materials (in insets). All materials deliver high capacities, typical for P2-type layered compounds. Ni-rich, $\text{Na}_{0.6}\text{Ni}_{0.22}\text{Fe}_{0.11}\text{Mn}_{0.66}\text{O}_2$ material reveals a first discharge capacity of 205 mAh g^{-1} and 178 mAh g^{-1} after 30 cycles, corresponding to a capacity retention of about 86%. Similarly, Ni-free $\text{Na}_{0.4}\text{Fe}_{0.33}\text{Mn}_{0.66}\text{O}_2$ shows a first delivered capacity of about 200 mAh g^{-1} and of 174 mAh g^{-1} after 30 cycles with a capacity retention of about 87%. Hence, the most relevant difference between the various samples in figure 2 seems to be the energy efficiency or potential at which the capacity is delivered, i.e. moving to higher values by increasing the Ni-content, thus suggesting that the Ni-rich sample $\text{Na}_{0.6}\text{Ni}_{0.22}\text{Fe}_{0.11}\text{Mn}_{0.66}\text{O}_2$ to provide higher energies. The cycling behaviour of the different materials in the first 30 cycles is similar to our previous observations for the long-term cycling of $\text{Na}_{0.5}\text{Ni}_{0.23}\text{Fe}_{0.13}\text{Mn}_{0.63}\text{O}_2$ at higher C-rate suggesting for similar long-term cyclability.³⁰

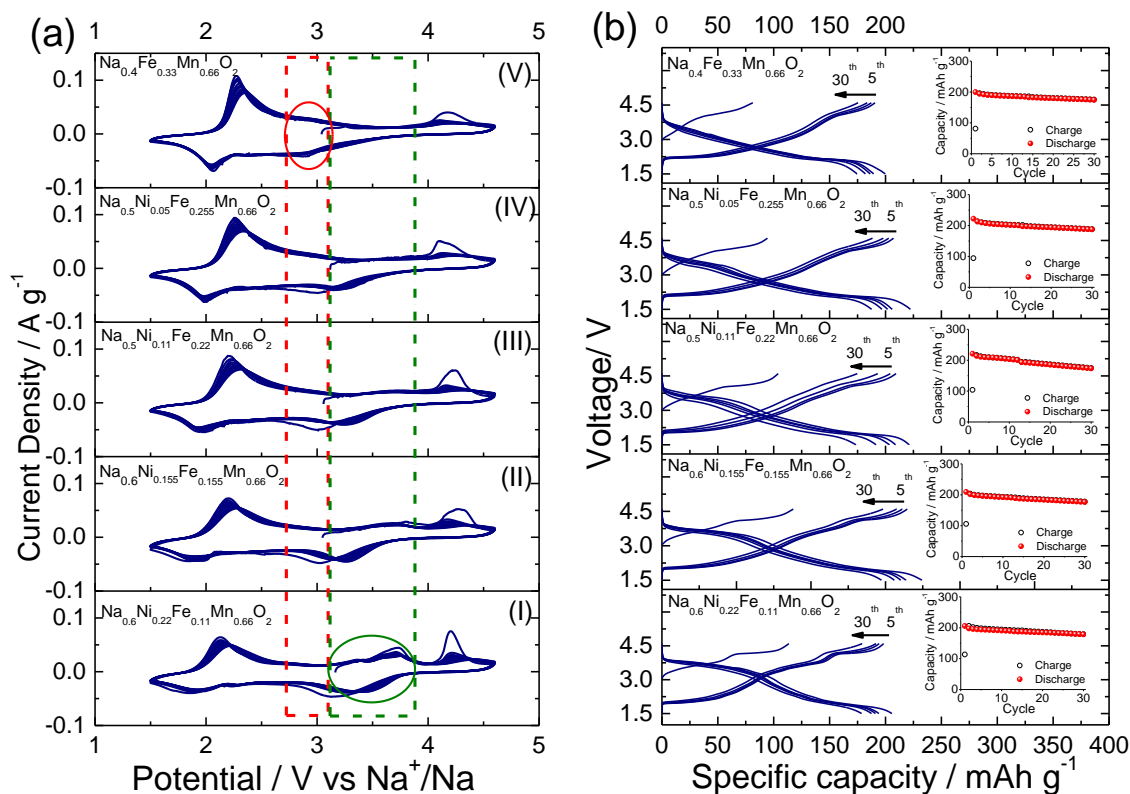


Figure 2. (a) Cyclic voltammetry test performed using P2-type layered materials obtained at 900 °C in sodium cells. (I)Na_{0.6}Ni_{0.22}Fe_{0.11}Mn_{0.66}O₂, (II)Na_{0.6}Ni_{0.155}Fe_{0.155}Mn_{0.66}O₂, (III)Na_{0.5}Ni_{0.11}Fe_{0.22}Mn_{0.66}O₂, (IV)Na_{0.5}Ni_{0.05}Fe_{0.255}Mn_{0.66}O₂ and (V)Na_{0.4}Fe_{0.33}Mn_{0.66}O₂. Tests performed using a scan rate of 0.1 mV sec⁻¹ within the 1.5–4.6 V potential range. Counter and reference electrode of Na. Temperature: 20°C±2°C. Electrolyte: 1M NaPF₆ in PC. (b) Cycling performances of the above mentioned electrodes in sodium cells in terms of voltage profiles and cycling behavior (inset). Tests run at 15 mA g⁻¹ within the 1.5–4.6 V voltage range. Counter and reference electrode of Na. Temperature: 20°C±2°C. Electrolyte: 1M NaPF₆ in PC.

Figure 3 reports the effect of annealing temperature (either 800°C, 850°C or 900°C) on the structural and electrochemical characteristics of the sample with the most promising performance, i.e. Na_{0.6}Ni_{0.22}Fe_{0.11}Mn_{0.66}O₂. The XRD pattern in Figure 3a, reveals the material prepared at 900 °C to be

of P2-type layered structure (space group: $P6_3/mmc$). The Rietveld refinement using the hexagonal unit cell leads to an intra-layer distance (M-M) of $a=2.88\text{\AA}$ and inter-layer distance of $c=11.2\text{\AA}$. The FE-SEM image reported as inset in Fig. 3a clearly shows the platelet like micrometric morphology, characterized by a sequence of smooth facets. The XRD pattern of the sample prepared at $850\text{ }^\circ\text{C}$ is reported in Figure 3b and reveals that the lower annealing temperature induces the formation of a new phase, i.e. P3. Indeed, the Rietveld refinement of the pattern indicates a mix of P2 and P3 phases, with about 40% content of the former phase. The material with P2-P3 structure reveals a different morphology, including the particle size. The FE-SEM image reveals a smaller sub-micrometric particles size for the mixed P2-P3 phase in comparison with the pure P2 phase. The NaNFM samples prepared at $800\text{ }^\circ\text{C}$ (Figure 3c), shows that a further decrease of the annealing temperature of $50\text{ }^\circ\text{C}$ leads to the formation of a pure P3-type structure with $R3m$ space group. The latter may be refined using the rhombohedral unit cell leading to an intra-layer distance (M-M) of $a=2.88\text{\AA}$ and inter-layer distance of $c=16.9\text{\AA}$, while the FE-SEM inset of Fig. 3c reveals nano-metric particle size.

The potential profiles of the first cycle as well as the capacities and corresponding coulombic efficiencies obtained during galvanostatic cycling are shown in Figure 3d for the different $\text{Na}_{0.6}\text{Ni}_{0.22}\text{Fe}_{0.11}\text{Mn}_{0.66}\text{O}_2$ samples. The $\text{Na}_{0.6}\text{Ni}_{0.22}\text{Fe}_{0.11}\text{Mn}_{0.66}\text{O}_2$ samples prepared at $800\text{ }^\circ\text{C}$, $850\text{ }^\circ\text{C}$ and $900\text{ }^\circ\text{C}$ reveal only a minor difference in terms of the first charge capacity (121 mAh g^{-1} , 110 mAh g^{-1} and 113 mAh g^{-1} , respectively). However, in the subsequent discharge process the delivered capacity differs significantly (234 mAh g^{-1} , 216 mAh g^{-1} and 205 mAh g^{-1} , respectively). These results might suggest the P3-type structured material, synthesized at the lower temperature, to exhibit the best overall electrochemical performance. However, the cycling behaviour reported as inset in Fig.3d clearly evidences the contrary. After 30 cycles a discharge capacity of 176 mAh g^{-1} , 129 mAh g^{-1} and 178 mAh g^{-1} is delivered for the pure P3-type ($800\text{ }^\circ\text{C}$), mixed P2-P3-type ($850\text{ }^\circ\text{C}$) and P2-type ($900\text{ }^\circ\text{C}$) material, corresponding to a capacity retention of 75%, 60% and 87%, respectively. These results clearly indicate

that the higher initial capacity is also interconnected with a higher capacity fade. Consequently, the most stable cycling behaviour is achieved by the P2-type structured layered oxide. The different electrochemical performances of the samples are most probably not originating from the different structure but rather induced by the morphological features and, in particular, the particle size. The P3 phase, characterized by remarkably smaller particles, shows a high initial capacity but pronounced fading upon cycling as well as lower efficiency (99.2%), while the P2 phase, characterized by bigger particles, evidences lower initial capacity, greater stability and higher efficiency (99.7%). In fact, it has been reported that the low stability of the P3 phase may be attributed to a more pronounced manganese dissolution, a phenomenon often present in Mn based layered materials and further accelerated by the presence of very small or nanosized particles.³⁶ Nevertheless, although this explains the different performance of the pure P2-type and P3-type phase, the mixed structure is clearly not revealing an intermediate but a much lower cycling stability, indicating a continuous active material degradation process to be present. In fact, this observation is in line with the results reported for mixed P2/P3-type $\text{Na}_x\text{Ni}_{0.22}\text{Co}_{0.11}\text{Mn}_{0.66}\text{O}_2$, in which a strong manganese dissolution was present in organic carbonate based electrolytes.³⁶ This somewhat indicates mixed P2/P3-type structured materials not being suitable active materials in this electrolytic solution.

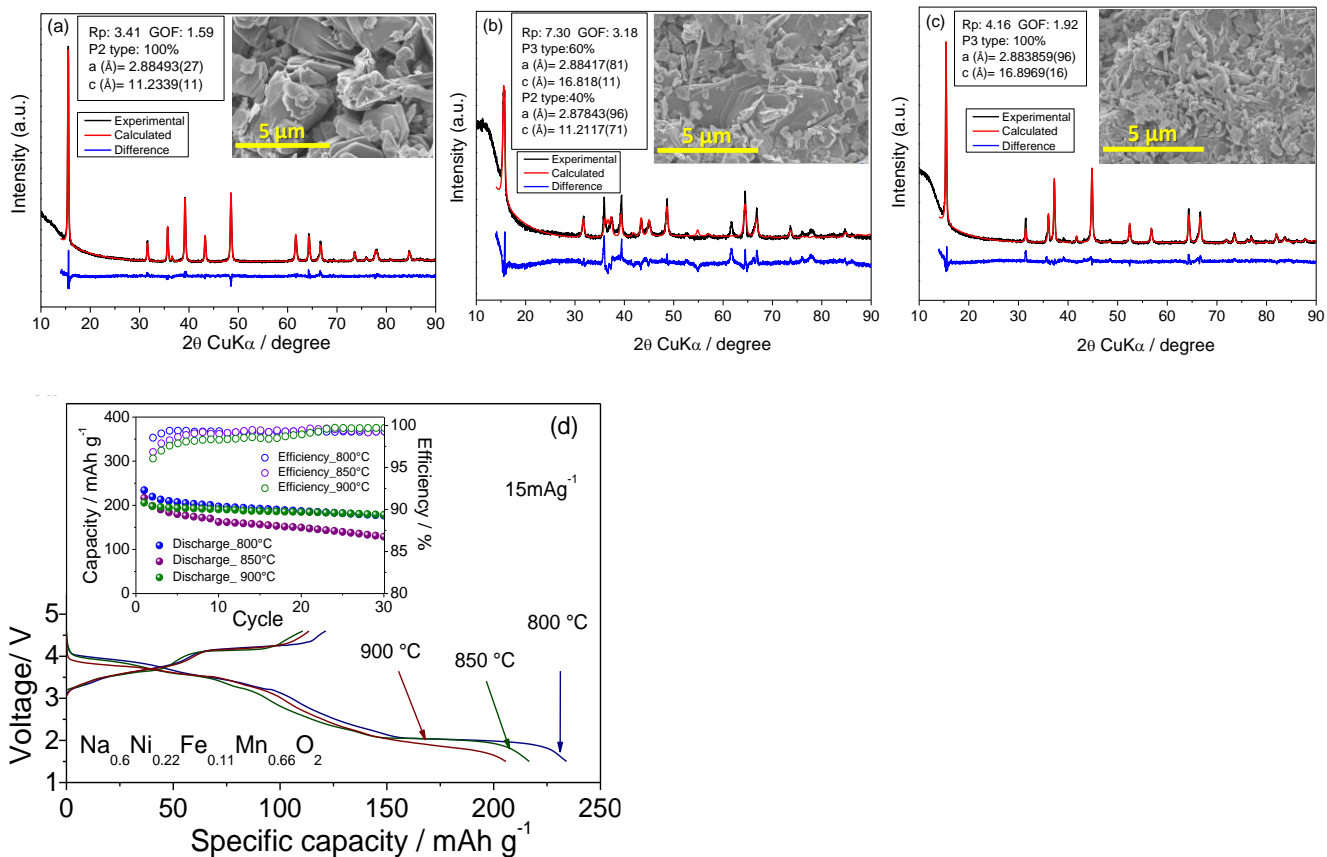


Figure 3. Experimental (black line) and calculated (red line) XRD diffraction patterns of a $\text{Na}_{0.6}\text{Ni}_{0.22}\text{Fe}_{0.11}\text{Mn}_{0.66}\text{O}_2$ material prepared using the annealing temperature of (a) 900 °C (pure P2), (b) 850 °C (mixed P2-P3) and (c) 800 °C (pure P3). Figure insets report the respectively Field Emission Scanning Electron Microscopy (FE-SEM) images. (d) Comparison of the first charge-discharge voltage profile (and inset of cycling behavior and efficiency) of sodium cells using the NFM compounds prepared at 900 °C, 850 °C and 800 °C, respectively. Tests run at 15 mA g⁻¹ within the 1.5–4.6 V voltage range. Counter and reference electrode of Na. Temperature: 20°C±2°C. Electrolyte: 1M NaPF₆ in PC.

The samples reported in figures 1, 2 and 3 were prepared by using a stoichiometric sodium content of 0.685 eq. during the synthesis. The stoichiometries of the final compounds, as detected by ICP, indicate a sodium content varying from 0.6 to 0.4 equivalent, suggesting partial loss of Na during the

temperature annealing and water rinsing processes. Figure 3 demonstrated the annealing at 900 °C to lead to the P2-type phase while annealing at 800 °C results into the P3 structure. However, in the following we demonstrate that a P2-type structure phase can be also obtained at the lower temperatures via increasing the stoichiometric sodium content. Figure 4 reports the measured and calculated XRD patterns of the layered $\text{Na}_x\text{Ni}_{0.22}\text{Fe}_{0.11}\text{Mn}_{0.66}\text{O}_2$ materials annealed at 800 °C and using either 0.685 eq. (a) and 1.0 eq. (b) of sodium. The sample prepared with lower sodium content crystallizes into a P3-structure (space group R3m), while the material using an excess of sodium reveals the typical P2-structure with space group P63/mmc. Figure 4 (c) and (d) illustrate the potential profiles, capacities and efficiencies obtained during galvanostatic cycling of the P3-NaNFM and P2-NaNFM electrodes, respectively. The P3- $\text{Na}_x\text{Ni}_{0.22}\text{Fe}_{0.11}\text{Mn}_{0.66}\text{O}_2$ electrode delivers 121 mAh g⁻¹ during the first charge and 234 mAh g⁻¹ in the following discharge, while the P2- $\text{Na}_x\text{Ni}_{0.22}\text{Fe}_{0.11}\text{Mn}_{0.66}\text{O}_2$ exhibits lower capacities of 113 mAh g⁻¹ and 208 mAh g⁻¹ during the first charge and discharge, respectively. Both materials show a good overall cycling behavior, but the better performance is evidenced by the P2-type layered electrode, as already demonstrated by figure 3 reporting the samples synthesized at various temperatures. In more detail, the P2-type material exhibits a slightly better energy efficiency of the (de-)sodiation process, higher coulombic efficiencies (99.3 vs. 99.1% for the P3-type analogue) and a much better capacity retention upon cycling (82.1% vs. 75.5% after 30 cycles). Thus, a higher sodium content in the synthesis allows a reduction of the annealing temperature, while still the P2-type material with the better intrinsic electrochemical properties can be obtained. This represents a remarkable results which might enable a further cost reduction for the synthesis of layered materials, as cost represents such an important issue for SIBs. The cathode materials here reported show an issue associated with sodium deficiency that may lead to sodium-ion full cell balance. This drawback may be mitigated by chemical or electrochemical activation process before the use of the electrodes in a full cell. Possible pre-activation of the anode

material leading to an extra amount of sodium may be performed by chemical sodiation procedure involving direct contact of the anode with sodium metal wet by the electrolyte prior its use in full cell.³⁷

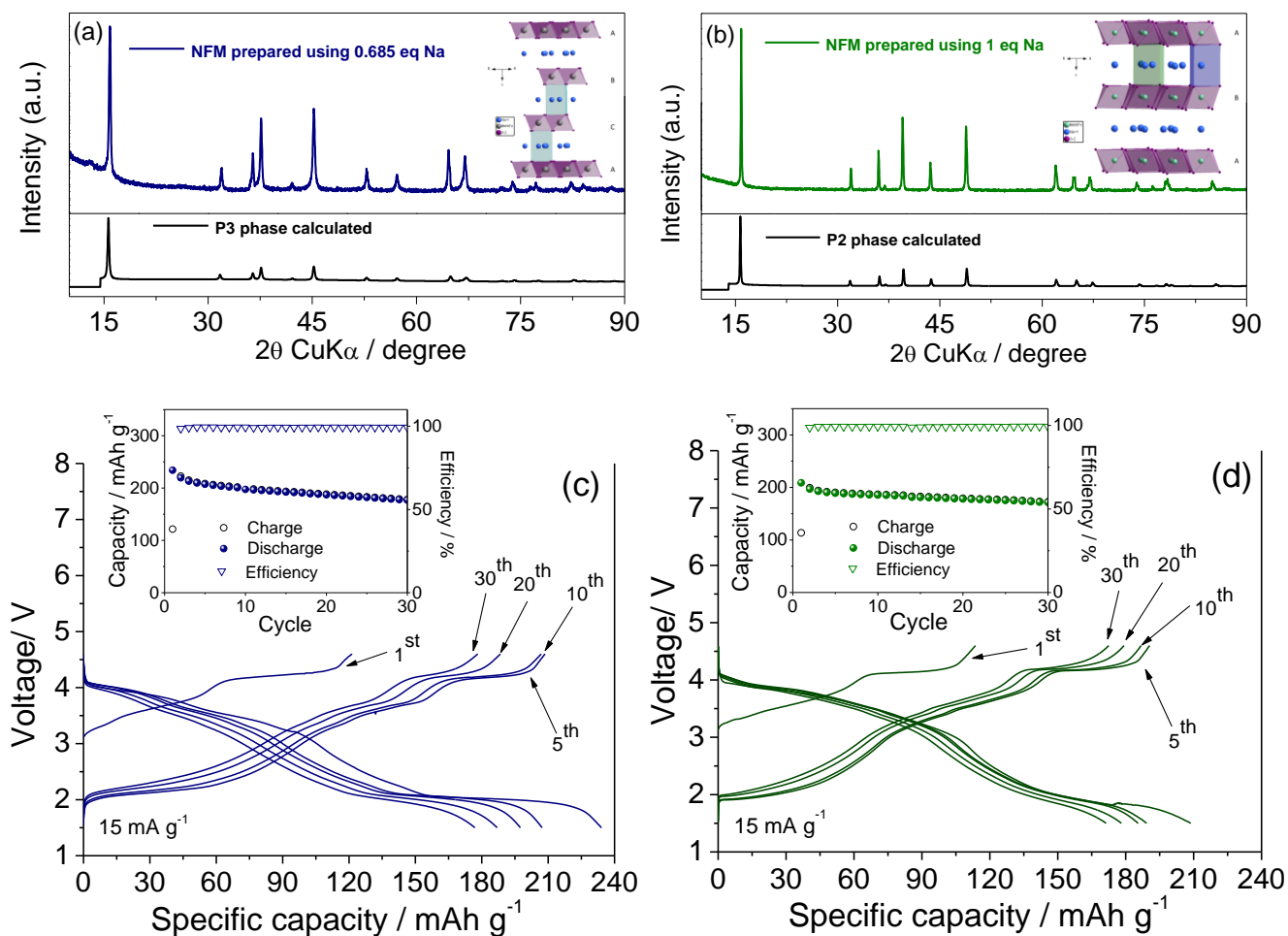


Figure 4. XRD diffraction patterns of $\text{Na}_x\text{Ni}_{0.22}\text{Fe}_{0.11}\text{Mn}_{0.66}\text{O}_2$ obtained at 800 °C with different amount of Na equivalent, i.e. 0.685 (a) and 1 (b). Voltage profiles and, in inset, cycle life of sodium cells using a $\text{Na}_x\text{Ni}_{0.22}\text{Fe}_{0.11}\text{Mn}_{0.66}\text{O}_2$ electrode obtained at 800 °C using 0.685 eq. Na (c) and 1eq. Na (d). Tests run at 15 mA g⁻¹ within the 1.5–4.6V voltage range. Counter and reference electrode of Na. Temperature: 20°C±2°C. Electrolyte: 1M NaPF₆ in PC.

Conclusion

In this work we reported a deep study on layered transition metal oxides Na_xMO_2 ($\text{M}=\text{Ni}, \text{Fe}, \text{Mn}$) for their use as cathode materials in sodium-ion batteries. The materials have been prepared through an optimized synthetic route involving co-precipitation method, an annealing process in air and a water-rinsing process. The effect of the Ni to Fe ratio, the annealing temperature and stoichiometric sodium content during the synthesis have been investigated as parameters affecting the electrochemical properties of the prepared oxides. We demonstrated via a comparative study that these factors play a crucial role for the materials structure and morphology, thus leading to a different electrochemical behavior. The data indicated that higher annealing temperatures (900°C , 0.685 eq. Na^+), as well as stoichiometric sodium content employed during the synthesis (800°C , 1.0eq. Na^+), promote P2-phase formation, while lower temperatures and lower sodium amount enable the formation of P3-type phase (800°C , 0.685 eq. Na^+). The reported results indicated that different Ni to Fe ratio only slightly affects the good electrochemical behavior of the P2-type layered electrodes in terms of delivered capacity, while the nickel content remarkably influences the working potential. Moreover, we demonstrated that increased Ni content in the transition metal layers can improve the energy efficiency of the (de)sodiation process and, finally, hinder the Mn dissolution. It has been demonstrated that P-type layered oxides, in particular Ni-rich ones, are suitable cathode materials for sodium-ion batteries in view of the high delivered capacities of about 200 mAh g^{-1} . Furthermore, the data evidenced that the well-defined structure and the favorable morphological properties of the P2-layered electrode allow better electrochemical performances in terms of cycling stability compared with the P3-type electrode.

Acknowledgments

IH and JH would like to thank the support of the Italian project “Regione Lazio” at Sapienza University of Rome, Chemistry Department. DB and SP acknowledges the financial contribution of BMW AG.

References

- (1) Scrosati, B. ; Hassoun, J. ; Sun, Y.-K. Lithium-ion Batteries. A Look into the Future *Energy Environ. Sci.* **2011**, *4*, 3287-3295.
- (2) Tarascon, J.-M.; Armand, M. Issues and Challenges Facing Rechargeable Lithium Batteries *Nature* **2001**, *414*, 359-367.
- (3) Tarascon, J.-M. Is Lithium the New Gold? *Nat. Chem.* **2010**, *2*, 510–510.
- (4) Jaskula, B.W. *Lithium*, in *Mineral Commodity Summaries 2012* , U. S. Geological Survey , Reston, VA 2012 , 94.
- (5) Palomares, V.; Serras, P.; Villaluenga, I.; Hueso, K.B.; Carretero-Gonzalez, J.; Rojo, T. Na-ion Batteries, Recent Advances and Present Challenges to Become Low Cost Energy Storage Systems *Energy Environ. Sci.* **2012**, *5*, 5884-5901.
- (6) Kim, S.-W.; Seo, D.-H.; Ma, X.; Ceder, G.; Kang, K. Electrode Materials for rechargeable Sodium-Ion Batteries: Potential Alternatives to Current Lithium-Ion Batteries *Adv. Energy Mater.* **2012**, *2*, 710–721.
- (7) Abraham, K. M. Intercalation Positive Electrodes for Rechargeable Sodium Cells *Solid State Ionics* **1982**, *7*, 199–212.
- (8) West, K.; Zachau-Christiansen, B.; Jacobsen, T.; Skaarup, S. J. Solid-state Sodium Cells - an Alternative to Lithium Cells *J. Power Sources* **1989**, *26*, 341–345.
- (9) Delmas, C.; Braconnier, J.J.; Fouassier, C.; Hagenmuller, P. Electrochemical intercalation of sodium in Na_xCoO_2 bronzes *Solid State Ionics* **1981**, *3–4*, 165–169.
- (10) Nagelberg, A.S.; Worrell, W. L. A Thermodynamic Study of Sodium-intercalated TaS_2 and TiS_2 *J. Solid State Chem.* **1979**, *29*, 345–354.

- (11) Komaba, S.; Yabuuchi, N.; Nakayama, T.; Ogata, A.; Ishikawa, T.; Nakai, I. Study of the Reversible Electrode Reaction of $\text{Na}_{1-x}\text{Ni}_{0.5}\text{Mn}_{0.5}\text{O}_2$ for Rechargeable Sodium-ion Battery *Inorg. Chem.* **2012**, *51*, 6211-6220.
- (12) Sathiya, M.; Hemalatha, K.; Ramesha, K.; Tarascon, J.-M.; Prakash, A.S. Synthesis, Structure, and Electrochemical Properties of the Layered Sodium Insertion Cathode Material: $\text{NaNi}_{1/3}\text{Mn}_{1/3}\text{Co}_{1/3}\text{O}_2$ *Chem. Mater.* **2012**, *24*, 1846-1853.
- (13) Lu, Z.; Dahn, J.R. In Situ X-Ray Diffraction Study of $\text{P2-Na}_{2/3}\text{Ni}_{1/3}\text{Mn}_{2/3}\text{O}_2$ *J. Electrochem. Soc.* **2001**, *148*, A1225-A1229.
- (14) Wu, L.; Bresser, D.; Buchholz, D.; Giffin, G.; Ramirez Castro, C.; Ochel, A.; Passerini, S. Unfolding the Mechanism of Sodium Insertion in Anatase TiO_2 Nanoparticles *Adv. Energy Mater.* **2014**, doi: 10.1002/aenm.201401142.
- (15) Ponrouch, A.; Goñi, A.R.; Palacín, M. Rosa High Capacity Hard Carbon Anodes for Sodium ion Batteries in Additive Free Electrolyte *Electrochem. Commun.* **2013**, *27*, 85-88.
- (16) Fouassier, C.; Delmas, C.; Hagenmuller, P. Evolution Structurale et Proprietes Physiques des Phases A_xMO_2 (A = Na, K; M = Cr, Mn, Co) ($x \leq 1$) *MRS Bull.* **1975**, *10*, 443-449.
- (17) Delmas, C.; Fouassier, C.; Hagenmuller, P. Structural Classification and Properties of Layered Oxides *Physica* **1980**, *99*, 8.
- (18) Kubota, K.; Yabuuchi, N.; Yoshida, H.; Dahbi, M.; Komaba, S. Layered Oxides as Positive Electrode Materials for Na-ion Batteries *MRS Bull.* **2014**, *39*, 416-422.
- (19) Hamani, D.; Ati, M.; Tarascon, J.-M.; Rozier, P. Na_xVO_2 as Possible Electrode for Na-Ion Batteries *Electrochem. Commun.* **2011**, *13*, 938-941.
- (20) Komaba, S.; Takei, C.; Nakayama, T.; Ogata, A.; Yabuuchi, N. Electrochemical Intercalation Activity of Layered NaCrO_2 vs. LiCrO_2 *Electrochem. Commun.* **2010**, *12*, 355-358.

- (21) Caballero, A.; Hernán, L.; Morales, J.; Sánchez, L.; Santos Peña, J.; Aranda, M.A.G. Synthesis and Characterization of High-temperature Hexagonal P2-Na_{0.6}MnO₂ and its Electrochemical Behaviour as Cathode in Sodium Cells *J. Mater. Chem.* **2002**, *12*, 1142–1147.
- (22) Yabuuchi, N.; Yoshida, H; Komaba, S. Crystal Structures and Electrode Performance of Alpha-NaFeO₂ for Rechargeable Sodium Batteries *Electrochemistry* **2012**, *80*, 716–719.
- (23) Vassilaras, P.; Ma, X.; Li, X.; Ceder, G. Electrochemical Properties of Monoclinic NaNiO₂ *J. Electrochem. Soc.* **2013**, *160*, A207–A211.
- (24) Su, D.; Wang, C.; Ahn, H.-j.; Wang, G. Single Crystalline Na_{0.7}MnO₂ Nanoplates as Cathode Materials for Sodium-Ion Batteries with Enhanced Performance *Chem. Eur. J.* **2013**, *19*, 10884 – 10889.
- (25) Su, D.; Wang, G. Single-Crystalline Bilayered V₂O₅ Nanobelts for High-Capacity Sodium-Ion Batteries *ACS Nano* **2013**, *7*, 11218–11226.
- (26) Su, D.; Ahn, H.-j.; Wang, G. β-MnO₂ Nanorods with Exposed Tunnel Structures as High-performance Cathode Materials for Sodium-ion Batteries *NPG Asia Mater.* **2013**, *5*, e70.
- (27) Ding, J.J.; Zhou, Y.N.; Sun, Q.; Yu, X.Q.; Yang, X.Q.; Fu, Z.W. Electrochemical Properties of P2-Phase Na_{0.74}CoO₂ Compounds as Cathode Material for Rechargeable Sodium-ion Batteries *Electrochim. Acta* **2013**, *87*, 388–393.
- (28) Yabuuchi, N.; Kajiyama, M.; Iwatate, J.; Nishikawa, H.; Hitomi, S.; Okuyama, R.; Usui, R.; Yamada, Y.; Komaba, S. P2-type Na_x[Fe_{1/2}Mn_{1/2}]O₂ Made from Earth-abundant Elements for Rechargeable Na Batteries *Nat. Mater.* **2012**, *11*, 512-517.
- (29) Buchholz, D.; Moretti, A.; Kloepsch, D.; Nowak, S.; Siozios, V.; Winter, M.; Passerini, S. Toward Na-ion Batteries-Synthesis and Characterization of a Novel High Capacity Na Ion Intercalation Material *Chem. Mater.* **2013**, *25*, 142-148.

- (30) Hasa, I.; Buchholz, D.; Passerini, S.; Scrosati, B.; Hassoun, High Performance $\text{Na}_{0.5}[\text{Ni}_{0.23}\text{Fe}_{0.13}\text{Mn}_{0.63}]\text{O}_2$ Cathode for Sodium-Ion Batteries *J. Adv. Energy Mater.* **2014**, doi:10.1002/aenm.201400083.
- (31) Lu, Z.; Dahn, J.R. Intercalation of Water in P2, T2 and O2 Structure $\text{A}_2[\text{Co}_x\text{Ni}_{1/3-x}\text{Mn}_{2/3}]\text{O}_2$ *Chem. Mater.* **2001**, *13*, 1252-1257.
- (32) Buchholz, D.; Gomes Chagas, L.; Vaalma, C.; Wu, L.; Passerini, S.; Water Sensitivity of Layered P2/P3- $\text{Na}_x\text{Ni}_{0.22}\text{Co}_{0.11}\text{Mn}_{0.66}\text{O}_2$ Cathode Material *J. Mater. Chem. A* **2014**, *2*, 13415–13421.
- (33) Lu, Z.; Donaberger, R.A.; Dahn, J.R. Superlattice Ordering of Mn, Ni, and Co in Layered Alkali Transition Metal Oxides with P2, P3, and O3 Structures *Chem. Mater.* **2000**, *12*, 3583–3590.
- (34) Yuan, D.; Hu, X.; Qian, J.; Pei, F.; Wu, F.; Mao, R.; Ai, X.; Yang, H.; Cao, Y. P2-type $\text{Na}_{0.67}\text{Mn}_{0.65}\text{Fe}_{0.2}\text{Ni}_{0.15}\text{O}_2$ Cathode Material with High-capacity for Sodium-ion Battery *Electrochim. Acta* **2014**, *116*, 300–305.
- (35) Thorne, J. S.; Dunlap, R.A.; Obrovac, M.N. Structure and Electrochemistry of $\text{Na}_x\text{Fe}_x\text{Mn}_{1-x}\text{O}_2$ ($1.0 \leq x \leq 0.5$) for Na-Ion Battery Positive Electrodes *J. Electrochem. Soc.* **2013**, *160*, A361-A367.
- (36) Gomes Chagas, L.; Buchholz, D.; Wu, L.; Vortmann, B.; Passerini, S. Unexpected Performance of Layered Sodium-ion Cathode Material in Ionic Liquid-based Electrolyte *J. Power Sources* **2014**, *247*, 377-383.
- (37) Lee, D.-J.; Park, J.-W.; Hasa, I.; Sun, Y.-K.; Scrosati, B.; Hassoun J. Alternative Materials for Sodium ion–sulphur Batteries *J. Mater. Chem. A* **2013**, *1*, 5256–5261

Table of content image

